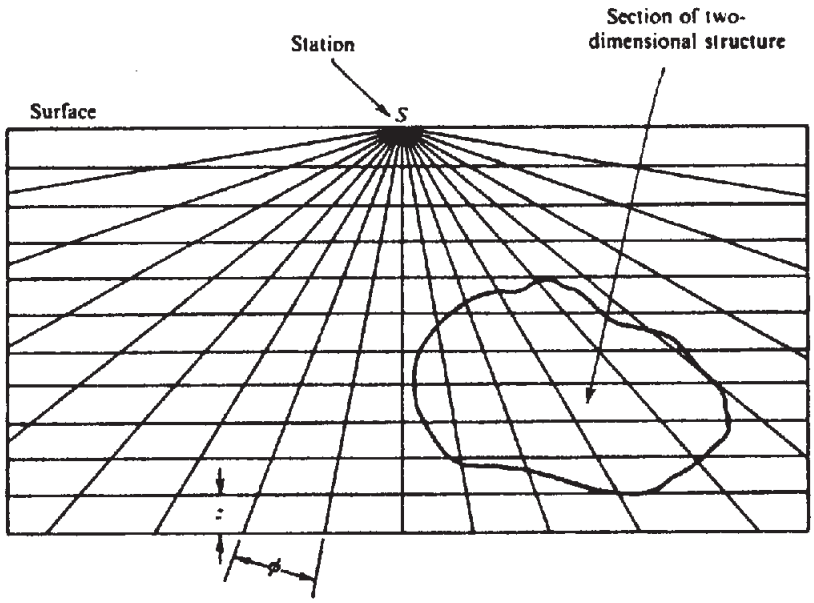

Figure 2.33. Template for calculating the gravity effect of two-dimensional bodies of irregular cross section. (From Hubbert, 1948).

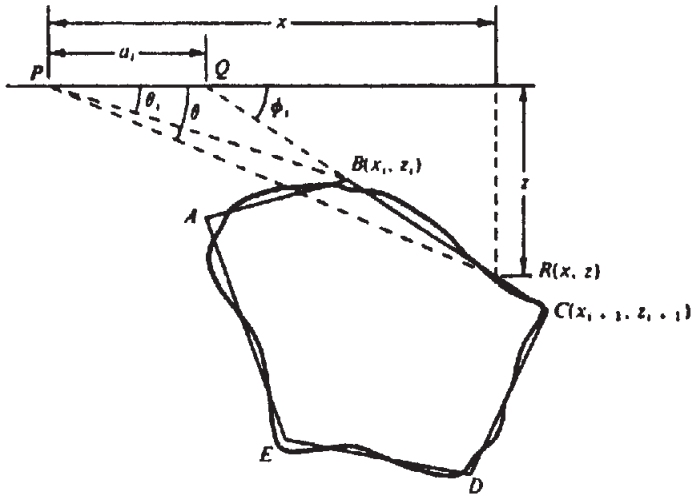

Figure 2.34. Polygon approximation of an irregular vertical section of a two-dimensional body.

computer, and then summing. This procedure is sometimes carried out graphically using templates superimposed on a cross section to divide it into elementary areas, each of which contributes the same effect at a surface station.

A template of this type is shown in Figure 2.33. The gravity effect at the chart apex is

$$g \approx K \times 10^{-5} \rho N \phi z \text{ mGal} \qquad (2.78)$$

where N is the number of segments covering the cross section, ϕ is the angular separation of radial lines, z is the separation of horizontal lines, $K = 23$ for z in meters and 7.1 for z in feet.

When the structure is not really two dimensional, the finite length can be taken into account by applying a correction. For a point in the plane of the cross section of a finite structure at a distance r from the section's center of gravity, the correction is

$$\frac{g}{g_m} = \frac{1}{2}\left\{\frac{1}{\left(1 + r^2/Y_1^2\right)^{1/2}} + \frac{1}{\left(1 + r^2/Y_2^2\right)^{1/2}}\right\} \qquad (2.79)$$

where g is the actual gravity of the finite body, g_m is the gravity for a body of the same cross section and of infinite length, and Y_1, Y_2 are the distances from the cross section to the ends of the body.

Graphical methods have also been employed on three-dimensional bodies by placing templates over

contours of the body in a horizontal plane. In effect, the body is broken up into a stack of horizontal slabs whose thickness is determined by the contour interval. This approach is more difficult than the two-dimensional procedure because the chart must have a variable scale parameter to allow for different slab depths.

One can calculate the gravity effect of a 2-D body of arbitrary cross section by using an n-sided polygon to approximate the outline of the vertical section (Talwani, Worzel, and Landisman, 1959). A simple section is illustrated in Figure 2.34. The gravity effect of this section is equal to a line integral around the perimeter (Hubbert, 1948). The relation is

$$g = 2\gamma\rho\oint z\, d\theta$$

From the geometry of Figure 2.34 we have the following relations:

$$z = x\tan\theta = (x - a_i)\tan\phi_i$$

or

$$z = (a_i \tan\theta \tan\phi_i)/(\tan\phi_i - \tan\theta)$$

The line integral for the side BC is

$$\int_{BC} z\, d\theta = \int_B^C \frac{a_i \tan\theta \tan\phi_i}{\tan\phi_i - \tan\theta}\, d\theta = Z_i$$

Thus,

$$g = 2\gamma\rho \sum_{i=1}^{n} Z_i \qquad (2.80)$$

In the most general case, Z_i is given by

$$Z_i = a_i \sin\phi_i \cos\phi_i \left[(\theta_i - \theta_{i+1}) + \tan\phi_i \cdot \ln\left\{\frac{\cos\theta_i(\tan\theta_i - \tan\phi_i)}{\cos\theta_{i+1}(\tan\theta_{i+1} - \tan\phi_i)}\right\}\right] \qquad (2.81)$$

where

$$\theta_i = \tan^{-1}\left(\frac{z_i}{x_i}\right), \qquad \phi_i = \tan^{-1}\left(\frac{z_{i+1} - z_i}{x_{i+1} - x_i}\right)$$

$$a_i = x_{i+1} - z_{i+1}\cot\phi_i = x_{i+1} + z_{i+1}\left(\frac{x_{i+1} - x_i}{z_i - z_{i+1}}\right)$$

This technique has also been used for three-dimensional bodies by replacing the contours in the horizontal plane with n-sided polygons. The solution, from line integrals of the polygons, is essentially a more complicated version of Equation (2.81).

2.7.9. The Direct and Inverse Problems of Interpretation

The interpretation techniques outlined in previous sections employ models with simplified shapes. Calculating the effects of models is the *direct* or *forward approach* to interpretation (the same procedure is used in other geophysical methods). The initial selection of a reasonable model is made with the aid of geological information and the experience of the interpreter. Interpretation in terms of simple models, a more-or-less force-fit to the data, is commonly used when data and control are incomplete. Detailed analysis is complicated by the fact that model fits are not unique. Ambiguity is well illustrated in the classic paper of Skeels (1947), who shows a gravity profile that could be produced by a number of mass distributions.

The inverse problem involves determining the geometry and physical properties of the source from measurements of the anomaly, rather than simply selecting a model and determining the parameters that match the anomaly approximately. The inherent nonuniqueness may make such a task appear to be a waste of time; however, with additional constraints and a computer, this type of analysis becomes increasingly useful.

We outline here a typical least-squares procedure for the inverse method. First, assume some mathematical model based on prior knowledge of the geology and/or of the geometry plus additional information gleaned from the general appearance of profiles and contours. Next, limit the number of parameters allowed to vary, for example, some subset of strike, length, attitude, depth, and depth extent; this makes the inverse problem more tractable. Next, linearize the problem (because the mathematical model is often essentially nonlinear) to simplify computations. Matrices (§A.2) are generally used. The solution is obtained by using the model and a given set of parameters to calculate simulated data (called the *model response*), comparing the model response with the values given by the observed data, and then varying the parameters to fit the data more closely. We illustrate this procedure as follows:

1. The model gives a relation between m parameters p_j. For each set of values of p_j, we get a model response $f(p_1, p_2, p_3, \ldots, p_m)$, which has a value $f_i(p_1, p_2, p_3, \ldots, p_m)$ at each of the n data points.

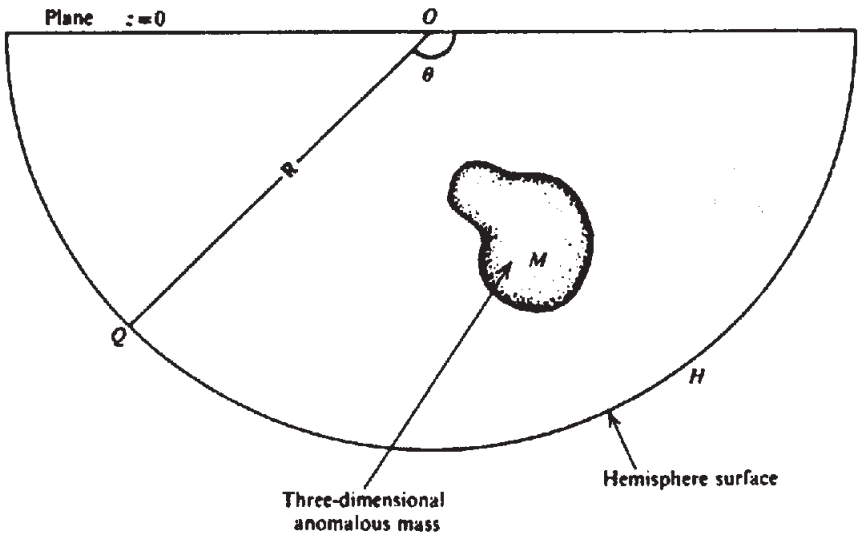

Figure 2.35. Calculation of excess mass.

We write

$$e_i = f_i(p_1, p_2, p_3, \ldots, p_m) - c_i \quad i = 1, 2, \ldots, n \tag{2.82}$$

where c_i are the observed data that f_i are intended to match and e_i are the errors between the observed data and the model response. We begin with an estimate of p_j.

2. Because $f(p_1, p_2, p_3, \ldots, p_m)$ generally involves nonlinear relations between the parameters, we simplify calculations by using a first-order Taylor-series expansion to get equations that are linear with respect to the derivatives. Differentiating Equation (2.82), we get

$$\sum(\partial f_i/\partial p_j)\,\delta p_j = \delta e_i \tag{2.83a}$$

where each derivative is evaluated using the current set of p_j values. In matrix notation Equation (2.83a) becomes

$$\mathcal{D}\mathcal{P} = \mathcal{E} \tag{2.83b}$$

where $\mathcal{D}$ is an $(n \times m)$ matrix whose elements are $\partial f_i/\partial p_j$, $\mathcal{P}$ is an $(m \times 1)$ column matrix of the sought-for parameter changes δp_j, and $\mathcal{E}$ is an $(n \times 1)$ column matrix whose elements are δe_i.

3. In the usual overdetermined case, $n \gg m$ and $\mathcal{D}$ is not square; we use Equation (A.5b) to solve Equation (2.83b):

$$\mathcal{P} = (\mathcal{D}^T\mathcal{D})^{-1}\mathcal{D}^T\mathcal{E} \tag{2.84}$$

This solution is equivalent to n equations in the m increments δp_j. Since $n > m$, we apply the method of least squares (Sheriff and Geldart, 1983, §10.1.5) to obtain the values of δp_j. The p_j are then replaced by $p_j + \delta p_j$ and the calculations are repeated. Iteration is stopped when Σe_i^2 is smaller than some acceptable (prespecified) value.

Many modifications of the preceding procedure exist, notably methods that stabilize the procedure. If $\mathcal{D}$ is too large to be efficiently handled by the computer, procedures such as steepest descent or conjugate gradient methods, may be employed. Marquardt (1963) employs an adjustable damping factor, whereas Jackson (1979) and Tarantola and Valette (1982) introduce a priori information to constrain the problem (see §3.8.2, example 3, for a similar magnetic procedure). If the model is highly nonlinear, these methods may not work well and Monte Carlo methods may be appropriate.

2.7.10. Excess Mass

Although there is no unique solution to a set of potential field data, it is possible to determine uniquely the total anomalous mass, regardless of its geometrical distribution. Sometimes this is a useful calculation (although potentially dangerous) in estimating ore tonnage in mineral exploration.

To find the *excess mass*, we start with Equation (2.12). Dropping the minus sign, we have

$$\int_S g_n\,ds = 4\pi\gamma M$$

We surround the mass by a hemisphere whose upper face is the datum plane $z = 0$. The surface integral can be separated into two parts: the integral over the

circular base in the xy plane and the surface of the half-sphere. From Figure 2.35, we have

$$\int_S g_n\,ds = \iint_{z=0} g_n\,dx\,dy + \iint_H g_n R^2 \sin\theta\,d\theta\,d\phi = 4\pi\gamma M$$

where g_n in the integral over the datum plane $z = 0$ is the residual anomaly $g(x, y)$ and R is the radius of the hemisphere. We take R large enough that M is in effect a point mass at the origin and $g_n = \gamma M/R^2$ at the hemispherical surface. Integration over this surface as ϕ goes from 0 to 2π and θ from $\pi/2$ to π leads to the value $2\pi\gamma M$, so that

$$\int_{-\infty}^{\infty}\int_{-\infty}^{\infty} g(x, y)\,dx\,dy = 2\pi\gamma M$$

or

$$M = (1/2\pi\gamma)\int_{-\infty}^{\infty}\int_{-\infty}^{\infty} g(x, y)\,dx\,dy \quad (2.85)$$

In practice, the integral is evaluated by numerical integration using the relation

$$M = K\sum g(x, y)\,\Delta x\,\Delta y \quad (2.86)$$

where m is in metric tons or short tons according as $K = 26.3$ for $\Delta x, \Delta y$ in meters, or $K = 2.44$ for $\Delta x, \Delta y$ in feet. The actual mass producing the anomaly can be determined if we know its density ρ_a and density contrast $\Delta\rho$. This multiplies Equation (2.86) by the factor $(\rho_a/\Delta\rho)$:

$$\text{actual mass} = (\rho_a/\Delta\rho) \times \text{excess mass} \quad (2.87)$$

If the regional has not been properly removed, or if other residual anomalies are included, the estimate obviously will be in error.

2.7.11. Overburden Effects

In many field situations, the effects of variations in the depth of the overburden may be larger than the effects of different rocks at depth, and so variations in overburden thickness can produce significant gravity anomalies. The average density for an assortment of overburden materials is about 1.92 g/cm^3 when wet and 1.55 g/cm^3 when dry, and the averages for wet and dry sedimentary rocks are ~ 2.50 and ~ 2.20 g/cm^3, respectively. Thus a contrast of 0.6 g/cm^3 is possible.

As a rough estimate, we expect the overburden to be thicker in valleys and low-lying flat land than on steep hillsides and elevated plateaus. Abrupt changes in overburden thickness, however, are common enough. In any gravity survey, and particularly in mineral exploration, it is worthwhile to consider the extent to which gravity anomalies may be caused by variations in overburden thickness.

From the Bouguer correction given in Equation (2.23) and the effect of a semiinfinite horizontal slab, we can get some idea of the magnitude of the overburden effect. The maximum gravity variation that results from a sudden change Δh in overburden thickness, where the density contrast is $\Delta\rho$, is given by

$$\Delta g_{max} = 41.9 \times 10^{-3}\,\Delta\rho\,\Delta h \quad (2.88a)$$

$$= 12.8 \times 10^{-3}\,\Delta\rho\,\Delta h' \quad (2.88b)$$

where Δh is in meters, $\Delta h'$ is in feet, and Δg_{max} is in milligals.

The maximum horizontal gradient of gravity will, of course, be large if overburden irregularity is the source. For abrupt depth changes of 10 m or more in a horizontal distance of 10 m and $\Delta\rho = 0.6$ g/cm^3, the value of (dg_{max}/dx) will be about 0.03 mGal/m. In fact, this steep gradient is more diagnostic than the magnitude of g_{max}. Clearly the depth of overburden should be measured in areas of shallow gravity anomalies. This is best done by small-scale refraction or surface resistivity measurements.

2.7.12. Maximum-Depth Rules

Smith (1959) gives several formulas for maximum depths of gravity distributions whose shapes are not known, provided that the anomalous bodies have a density contrast with the host rock that is either entirely positive or entirely negative. If $|g_{max}|$ and $|(\partial g/\partial x)_{max}|$ are the maximum values of gravity and of the horizontal derivative, respectively, the depth to the upper surface has a limiting value given by

$$z \le 0.86|g_{max}|/|(\partial g/\partial x)_{max}| \quad (2.89)$$

If the anomaly is two dimensional, the factor 0.86 becomes 0.65 in Equation (2.89). However, this expression is not particularly accurate.

2.8. FIELD EXAMPLES

(1) Figure 2.36a shows a Bouguer gravity contour map compiled from a survey in the vicinity of Portland Creek Pond in northern Newfoundland. This was an exploration program for oil and gas in

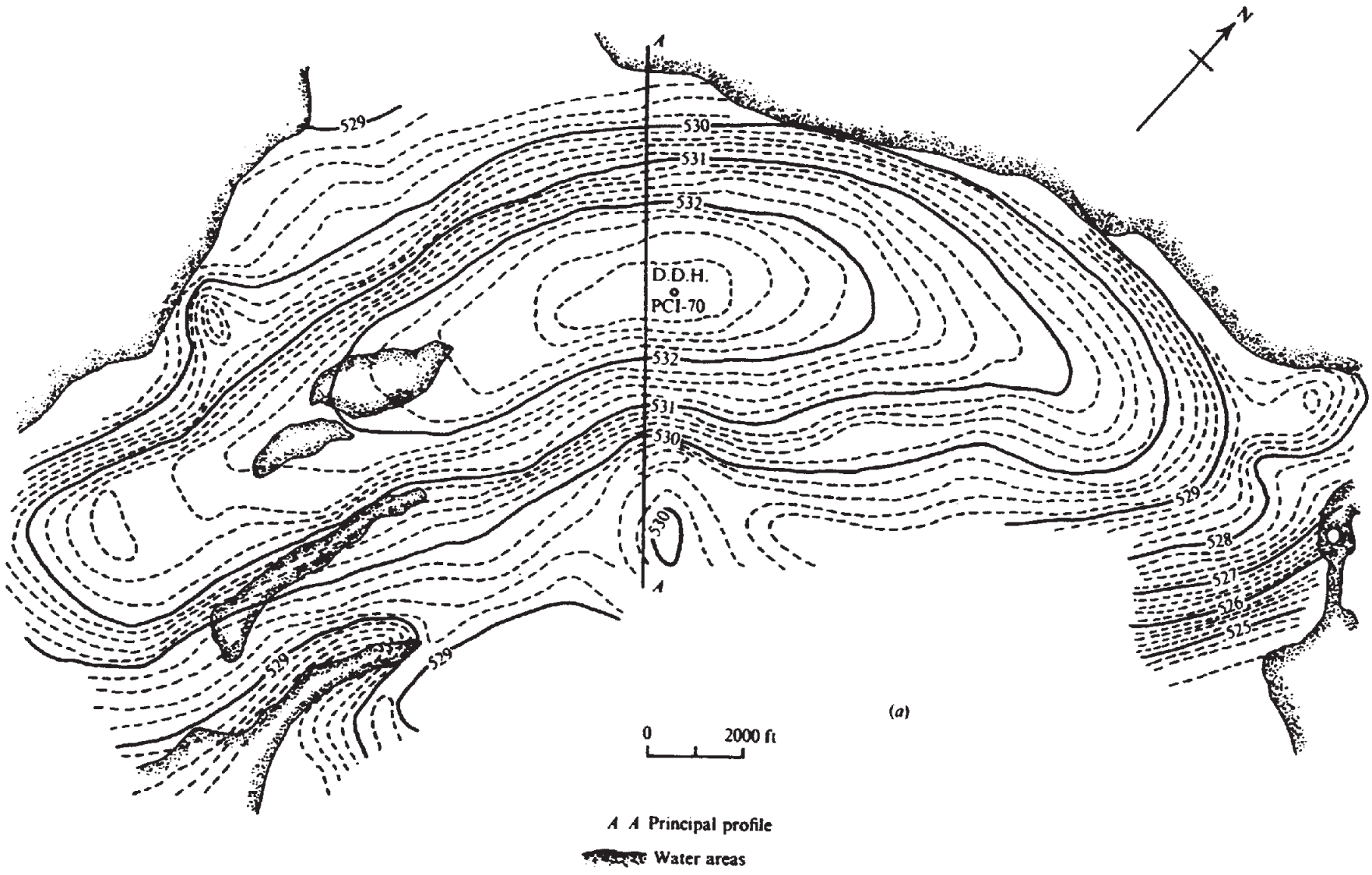

Figure 2.36. Gravity survey, Portland Creek Pond, Newfoundland. (a) Bouguer gravity map, contour interval (C.I.) = 0.2 mGal.

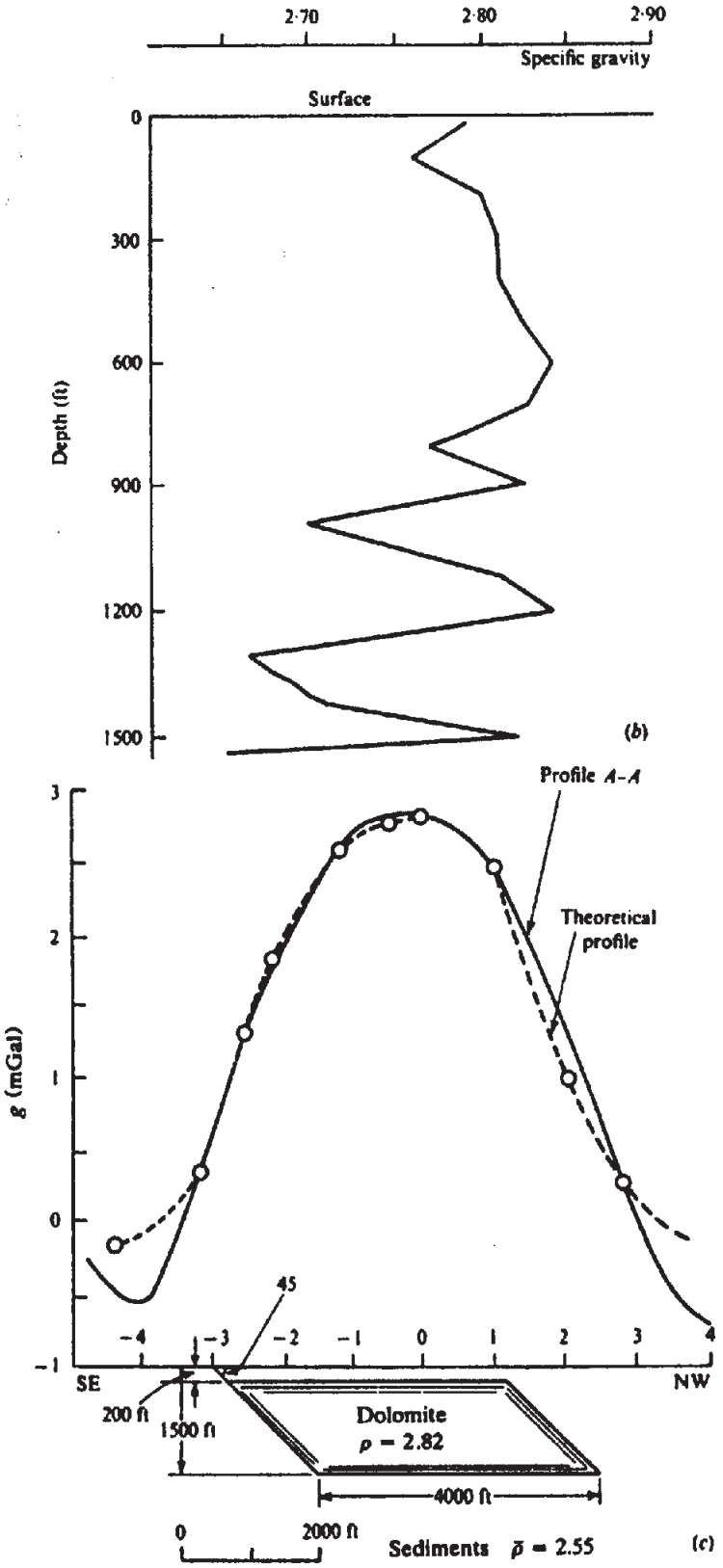

Figure 2.36. (Continued) (b) Density log in borehole DDH PCI-70. (c) Comparison with calculated profile for a 2-D dipping prism.

an area of sedimentary rocks whose thickness, a few miles south, is known to be over 5,000 ft. The topography is reasonably flat and no terrain corrections were required.

It is evident that the large positive anomaly is not a reflection of deep basement structure because the gradients are too steep. If we use Equation (2.68) to approximate a slab for profile AA' in Figure 2.36a, the values of g_{max} and $(\partial g/\partial x)_{max}$ indicate that h is not greater than 650–800 ft. This indicates that the source is shallow and hence must be within the sediments. One possibility is an intrusive dike of

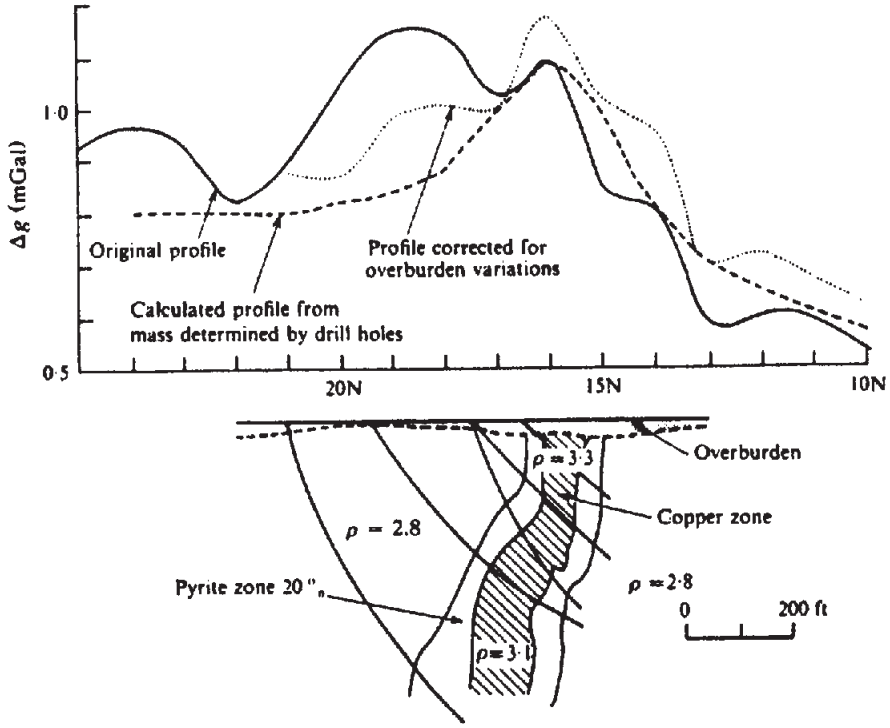

Figure 2.37. Gravity profiles over a copper deposit, Louvicourt, Quebec.

great linear extent, but Equation (2.74) shows that the flanks of the anomaly in this case would be much less steep than the field profile; this suggests that the source is of limited depth.

A 1,600 ft drill hole was put down in the center of this gravity anomaly; its location is shown in Figure 2.36a. Density measurements on core samples at 100 ft intervals are shown in Figure 2.36b. The local presence of dolomite from near surface to 1,000 ft and interbedded with dark shales from 1,000 to 1,600 ft accounts for the positive gravity. The average density of the dolomite samples was 2.82 g/cm^3. If the surrounding sedimentary formations are assumed to have a density of about 2.55 g/cm^3, it is possible to match the field profile reasonably well with the dipping prism shown in Figure 2.36c. This analysis is oversimplified since the actual structure is neither two dimensional ($L \approx 9b$) nor homogeneous in the bottom 500 ft. Both factors would steepen the flanks on the profile.

(2) The profiles in Figure 2.37 illustrate the pronounced effect of overburden thickness on gravity results. This is the Louvicourt Township copper deposit near Val d'Or, Quebec. Discovery was made by drilling a weak Turam anomaly (§7.4.3b); the gravity survey was carried out immediately after.

The original Bouguer gravity profile indicated a weak anomaly of 0.15 mGal directly over the conductor and a much broader and larger magnitude anomaly about 75 m to the north. Obviously the small peak would not have aroused any great enthusiasm. Later, when it had been established that the overburden thickness increased appreciably immediately over the sulfide zone, it was possible to correct for this variable thickness, as discussed in Section 2.7.11, using a density contrast of about 0.08 g/cm^3 between the host rock and the overburden. This is equivalent to 0.03 mGal/m of overburden thickness. In the corrected field profile the larger anomaly to the north has practically disappeared and the small peak has been enhanced to 0.3 mGal. A third profile calculated from density measurements of diamond drill cores is also shown.

This example clearly indicates the importance of measuring the overburden thickness in conjunction with gravity applied to small-scale mineral exploration. This is particularly necessary in surveys for vein-type base-metal deposits that respond to EM methods. The overburden effect would be less pronounced in regions favorable for IP, that is, large-area low-grade disseminated mineralization.

(3) The Delson fault is a well-documented structural feature in the St. Lawrence lowlands. Striking roughly E–W, it is located east of the St. Lawrence River several kilometers southeast of Montreal. Although the area is generally covered by about 15 m of overburden, there are exposures of Utica shales and Chazy limestones in river beds to indicate the location and direction of the fault. The sedimentary beds of the lowlands are flat-lying shales, limestones, and dolomites of Paleozoic age underlain by Precambrian basement rocks at a depth usually greater than 750 m.

Figure 2.38 shows a Bouguer gravity profile taken across the Delson fault in a N–S direction, together with a geologic section. A linear regional trend of

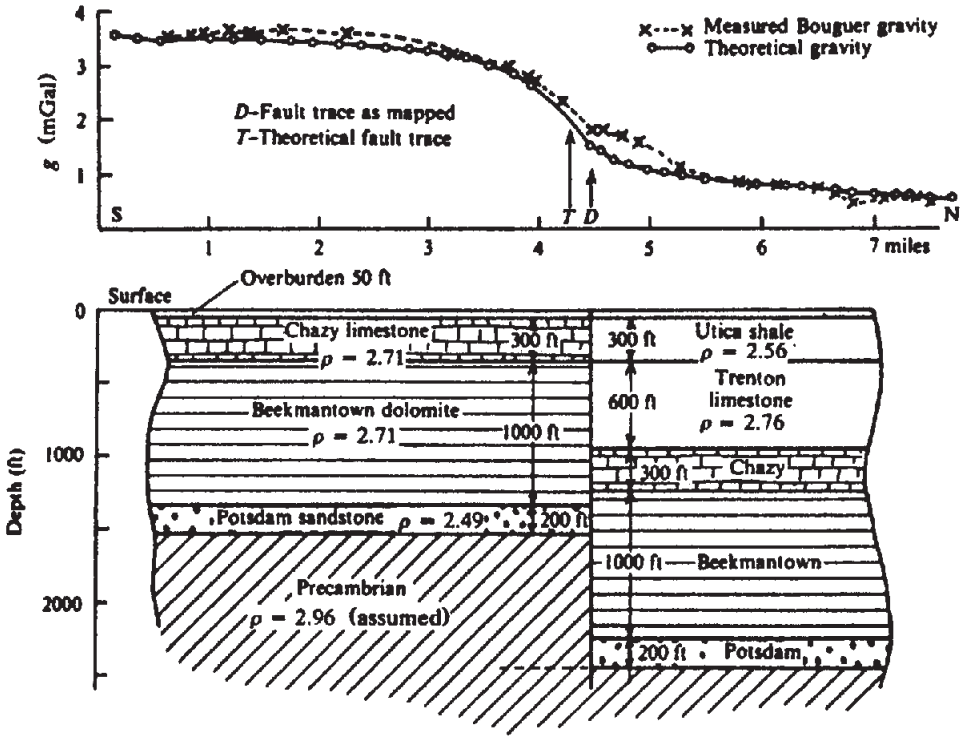

Figure 2.38. Gravity profile and geologic section across the Delson fault, St. Lawrence lowlands.

0.45 mGal/km positive to the south, has been removed.

The profile in Figure 2.38 resembles the gravity effect of a horizontal slab rather than a fault (compare with Figs. 2.28, 2.29, and 2.32). The only appreciable gravity effect from the sedimentary beds would be provided by the juxtaposition of the Chazy and Utica formations near surface and the displaced Potsdam layer (whose thickness is in some doubt) at greater depth. The first pair produces a gravity profile of the proper shape with a total variation of 0.57 mGal and maximum slope of 3.7 mGal/km; thus the total anomaly is too small and the slope too large to fit the field profile. The low-density Potsdam section, on the other hand, would tend to reduce the anomaly, since the bed nearer the surface lies on the south side of the fault; the total effect, however, is only about -0.1 mGal and maximum slope -0.15 mGal/km.

By postulating a density of 2.96 g/cm^3 in the Precambrian rocks and a step of 275 m on the fault down to the south, we obtain a total anomaly of 2.1 mGal with maximum slope of 1.2 mGal/km. The theoretical profile in Figure 2.38 is the result.

The theoretical profile is shifted about 300 m south of the mapped fault location. There are two explanations for this. First, the Delson fault is not vertical, but dips north about 80°. Second, faults very rarely show single clear-cut faces, that is, there is a faulted region of some width. The field profile also shows a small anomaly about $2\frac{1}{2}$ miles north of the Delson fault, although there is no supporting geological evidence.

2.9. PROBLEMS

1. Verify Equation (2.8). [*Hint:* Start with Equation (2.6a), integrate along the y axis between the limits $\pm L$, and subtract the potential at $(x^2 + z^2) = a^2 = 1$ (this avoids $U \to \infty$ as $L \to \infty$). By setting $L = \infty$, we get Equation (2.8).]
2. Show that Equation (2.12a) holds for an arbitrary closed surface S regardless of the position of m within S. [*Hint:* Write the integrand in the form $\gamma m(ds \cos\theta/r^2) = \gamma m\, d\Omega$, where r is the distance from m to ds, θ is the angle between $\mathbf{r}$ and $\mathbf{n}$, the outward-drawn normal to ds, and $d\Omega$ is the element of solid angle subtended by ds at m. Consider the case where $\mathbf{r}$ cuts S more than once.]
3. Verify Equations (2.62) and (2.63). [*Hint:* A solution of Equation (2.11c) is (Pipes and Harvill, 1970, p. 348)

$$g(r,\theta) = 2\pi\gamma\rho\left\{\sum_{n=0}^{\infty} a_n r^n + \sum_{n=0}^{\infty} b_n r^{-(n+1)}\right\} P_n(\mu)$$

where $\mu = \cos\theta$. When $r > z > R$, we use the

Table 2.3.

Stn	Time (hr)	g_{obs} (mGal)	Stn	Time (hr)	g_{obs} (mGal)	Stn	Time (hr)	g_{obs} (mGal)
Aug. 31	Line 0							
0°53	13:55	182.78	42	14:29	182.95	31	15:07	184.48
52	14:00	182.77	41	14:31	183.06	32	15:10	184.81
51	14:04	182.73	40	14:35	183.15	33	15:12	184.53
50	14:07	182.92	0°39	14:37	183.13	34	15:14	184.33
49	14:10	183.05	25	14:50	183.82	35	15:16	184.17
48	14:15	183.19	26	14:52	183.97	36	15:19	184.03
47	14:17	182.99	27	14:55	183.99	37	15:22	183.73
46	14:20	182.88	28	14:59	183.96	38	15:25	183.38
45	14:22	182.89	29	15:01	184.25	0°39	15:27	183.35
44	14:25	182.85	30	15:05	184.48	0°53	15:45	183.01
43	14:27	182.91						
Sept. 6	Line 2S							
0°53	9:10	185.02	33	10:56	185.39	44	11:44	184.53
2S°53	9:20	185.11	34	11:00	185.39	45	11:47	184.56
2S°39	9:40	184.93	35	11:05	185.52	46	11:52	184.64
24	10:19	185.86	36	11:09	185.37	47	11:55	184.67
25	10:23	185.66	37	11:15	185.00	48	11:59	184.67
26	10:27	185.65	38	11:20	184.86	49	12:02	184.76
27	10:31	185.66	2S°39	11:25	184.86	50	12:05	184.76
28	10:34	185.59	40	11:29	184.79	51	12:08	184.80
29	10:38	185.47	41	11:32	184.69	52	12:12	184.90
30	10:41	185.51	42	11:35	184.67	2S°53	12:16	185.09
31	10:45	185.46	43	11:39	184.60	0°53	12:28	185.03
32	10:50	185.39						

right-hand series and compare it with the expansion of Equation (2.60) in terms of (R/z) [see Eq. (A.43)] for points on the axis where $\mu = 1$, $P_n(1) = 1$, and $r = z$; this gives the values of b_l and we get Equation (2.62). Doing the same for $R > r > z$ and using the first series, we get Equation (2.63). Since $r > z$ on physical grounds, there are, in fact, only two cases: $r > R$ and $R > r$, so Equation (2.62) holds for the third case, $r > R > z$.]

4. The data in Table 2.3 were obtained over a 2 day period of gravity followup on a base-metal prospect. Stations marked ° were visited at least twice for drift correction. For example, station 53, line 0, was occupied at the beginning and end of each of the 2 days, station 53, line 2S, at the beginning and end of the second day's work and the stations 39 on both lines were used as base stations for checking drift at intermediate times.

   Draw a drift curve for the 2 day period and correct all station readings. (Note that each of the four stations 53 and 39 must have the same gravity readings – or very nearly so – as a result of the drift corrections.)

5. The gravity data in Table 2.4 were obtained during a followup on a small sphalerite showing in eastern Ontario. Reduce the gravity readings by taking out the drift, free-air (including height of instrument), Bouguer (assuming an average density of 2.67 g/cm^3), and latitude corrections (lines are N–S). Plot the two profiles. Are there any indications of a small high-grade (10–15%) or larger low-grade (2–5%) sphalerite deposit? Can you suggest any reason for the general shape of the profiles?

6. Show that the gravity anomaly produced by a vertical cone at its apex is

$$\Delta g_{max} = 2\pi\gamma\rho h(1 - \cos\alpha)$$

where h is the vertical height and α half the apex angle of the cone. Hence show that the terrain correction at the apex of a conical hill is

$$\delta g_t = 2\pi\gamma\rho h \cos\alpha$$

If $h = 1000$ ft, $\alpha = 68°$, and $\rho = 2.67$ g/cm^3, with the aid of a template and Table 2.1 determine the terrain correction required at various points on the sloping sides and on flat ground surrounding the cone (obviously the correction is the same at any particular elevation because of symmetry). How close to the base can gravity measurements be made without a significant terrain effect?

Table 2.4.

Stn L 8W	g_{obs} (mGal)	Time (PM)	H.I. (ft)	Elev. (ft)	Stn L 8W	g_{obs} (mGal)	Time (PM)	H.I. (ft)	Elev. (ft)
°3S	37.04	2.20	1.42	0.00	1 + 75	36.86	3.33	1.42	1.60
3 + 25	36.82	2.30	1.25	3.69	1 + 50	36.88	3.37	1.58	1.84
3 + 50	36.87	2.33	1.33	3.63	1 + 25	37.49	3.42	1.33	−5.81
3 + 75	36.84	2.36	1.33	4.78	1S	37.77	3.45	1.08	−9.68
4S	36.80	2.40	1.33	5.85	0 + 75	38.00	3.49	1.10	−13.99
4 + 25	36.68	2.45	1.33	7.11	0 + 50	38.03	3.53	0.83	−14.93
4 + 50	36.63	2.48	1.50	8.26	0 + 25	38.07	3.59	0.83	−15.06
4 + 75	36.57	2.52	1.17	10.03	B.L.	38.03	4.02	1.17	−15.30
5S	36.47	2.55	1.33	11.42	L 10W				
5 + 25	36.56	2.57	1.25	10.19	B.L.	37.62	4.23	1.42	−3.06
5 + 50	36.67	3.00	1.33	8.91	1S	37.94	4.34	1.08	−7.41
5 + 75	36.67	3.04	1.33	8.21	2S	37.60	4.38	1.23	−9.14
6S	36.73	3.06	1.42	7.46	3S	37.55	4.40	1.42	−8.20
°3S	37.06	3.13	1.33	0.00	4S	37.27	4.46	1.42	−4.85
2 + 75	36.96	3.17	1.33	−0.76	5S	37.45	4.50	1.17	1.04
2 + 50	36.74	3.23	1.42	1.18	6S		4.53	1.42	−1.04
2 + 25	36.89	3.28	1.25	1.23	L 8W				
2S	36.86	3.30	1.42	1.39	°3S	37.10	5.00	1.17	0.00

Note: L = line; B.L. = base line = 0 ft on each line; 3S = 300 ft south of base line, 3 + 75 = 375 ft south of base line, and so on; H.I. = height of instrument (gravimeter) above the surface whose elevation is given. Lat. of B.L. = 46°25'N.

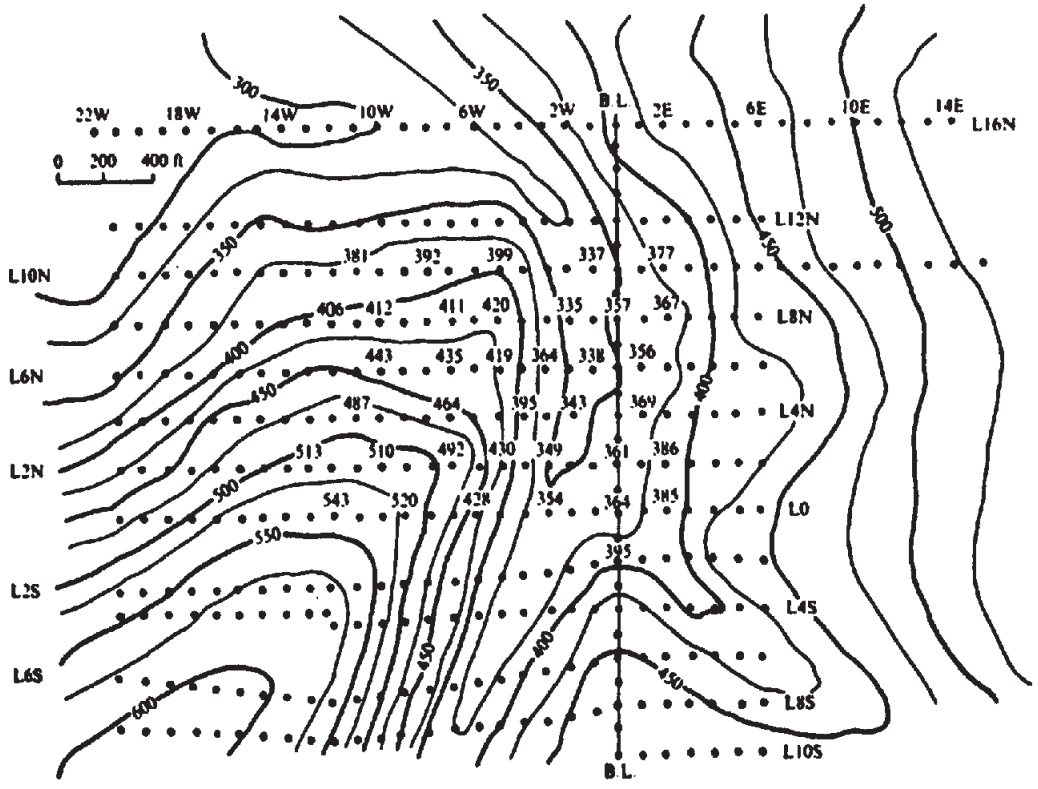

Figure 2.39. Topographic map for terrain correction.

7. The topographic map in Figure 2.39 was prepared in considerable detail to take out a terrain correction for a gravity survey. Make a template of appropriate scale for the first four or five zones of Table 2.1 (zones B–F) and calculate the terrain correction at several stations, such as (2N, 3W), (8N, 12W), (0, 9W), etc. Assuming that the topography is reasonably flat in the area surrounding the section illustrated, how many additional zones would be necessary to make a complete terrain correction?

In fact, there is a steep ridge to the northwest, striking southwest–northeast. At a distance of about 2 miles from the center of the area the

elevations increase from 300 to 1,100 ft within 1/2 mile. There is also a lake, which is roughly 1 mile across and a maximum of 100 ft in depth, situated about 2 miles to the northeast. To what extent would these large topographic features affect the overall terrain correction?

8. The reduced gravity readings (Bouguer) in Table 2.5 were obtained from an east–west traverse with stations at 30 m intervals. An electromagnetic survey carried our earlier had outlined a conducting zone about 750 m long, striking roughly north–south, with a maximum width of 50 m in the central part of the area. The gravity work was done as an attempt to assess the metallic content of the conductor. Four additional parallel gravity traverses, on lines adjacent to line 81N, produced essentially similar results. No information is available on the depth of overburden. Plot the profile and make a qualitative interpretation of the nature of the conducting zone based on the gravity survey.
9. The Bouguer gravity readings in Table 2.6 are taken from a survey in the sedimentary Pine Point area of the Northwest Territories. Station spacing is 30 m on a N–S line.

   Plot the profile and interpret the gravity anomaly, assuming it to be approximately two dimensional. Make two interpretations, assuming first that (a) below is valid, then assuming that (b) [but not (a)] is valid.

   (a) A Turam survey has not located any conductors in the area, while soil geochemistry shows minor lead and zinc.

   (b) The gravity anomaly coincides with a strong IP anomaly.

   Attempt to match the gravity profile with a simple geometrical cross section with particular regard to its depth, depth extent, and width.

Table 2.5. *Line 81N.*

Stn	g_B (mGal)	Stn	g_B (mGal)
85E	1.35	93E	0.77
86	1.30	94	0.75
87	1.25	95	0.66
88	1.22	96	0.55
89	1.20	97	0.51
90	1.15	98	0.50
91	1.07	99	0.40
92	0.87		

Table 2.6.

Stn	g_B (mGal)	Stn	g_B (mGal)
8S	0.02	2N	0.62
7S	0.06	3N	0.79
6S	0.08	4N	0.82
5S	0.09	5N	0.82
4S	0.08	6N	0.67
3S	0.06	7N	0.33
2S	0.01	8N	0.22
1S	0.04	9N	0.20
B.L.	0.19	10N	0.18
1N	0.41	11N	0.16

10. Residual gravity contours obtained from a survey over a base-metal area are shown in Figure 2.40. A regional trend of about 0.8 mGal/1,000 ft was removed to produce this map. A profile along the south–north line has also been plotted. The gravity anomaly is obviously caused by a plug-type of structure of considerable positive density contrast. Make an interpretation of the source as precisely as possible with these data.

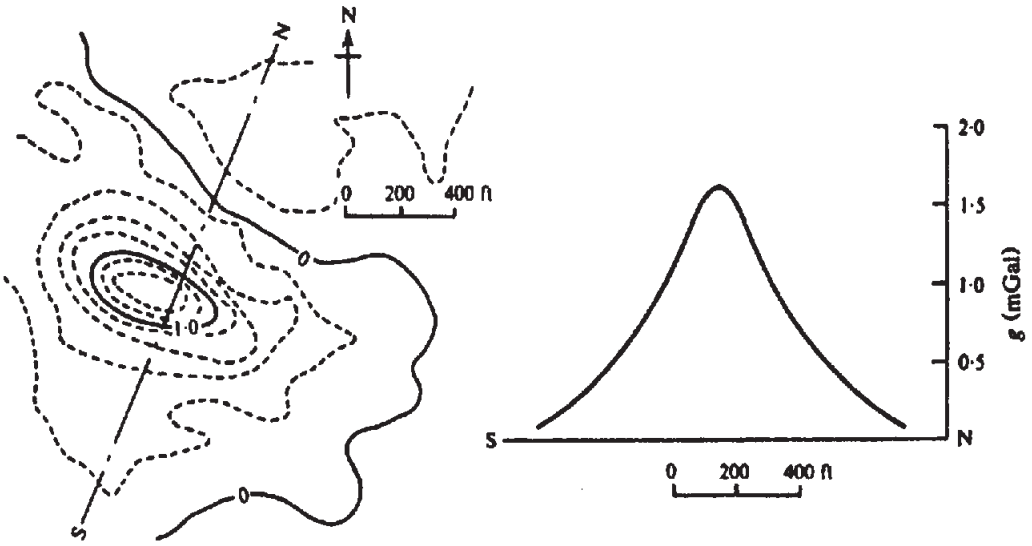

Figure 2.40. Residual gravity contours and principal profile, northwest Quebec.; C.I. = 0.2 mGal. (After Seigel, 1957.)

11. Table 2.7 gives Bouguer gravity readings from a survey made in the Bathurst area of northern New Brunswick. Station spacing is 100 ft and the line spacing is as noted. (L20N means 2,000 ft north of the base line.) Because of limited time and money, only four lines were selected for a followup of an earlier combined magnetic-electrical-geochemical survey. (Although this type of spot gravity work is used to some extent in base-metal exploration, it has obvious limitations.) There is a pronounced regional gradient, positive to the east, but it is not uniform, being stronger in the north lines and weakest on line 10N. Furthermore the large and irregular spacing between the lines makes it difficult to plot well-defined contours. On the other hand, if we attempt to remove the gradients from each line independently, it is not clear what background level should be selected; because we are looking for massive sulfides, the tendency is to overemphasize positive gravity areas. No measurements were made of overburden depth.

    Try to remove the regional by graphical smoothing and by gridding (more sophisticated techniques are not warranted). Interpret any remaining residuals.

12. Additional data obtained in the gravity survey of problem 4 are given in Table 2.8. Lines are east–west, 200 m apart; stations are 50 m apart with the larger numbers to the west. For some reason the base line through Stn 0 was cut at an angle of 20° east of true north, so that each station on line 0 is displaced about 73 m east of its equivalent on line 2S. Obviously there is a small latitude correction, 2ϕ being $\approx 93°$.

    Using the data in problem 4 (corrected for drift), apply the appropriate reductions to obtain Bouguer gravity for all stations, using an average density of 2.67 g/cm^3 for the local formations which consist of gneiss on the western portion extending roughly to station 25 and ultrabasic rocks to the east. There are frequent large outcrops in the eastern region, while the gneiss is covered by a fairly uniform thin overburden of 1–2 m. Plot the gravity profiles and make an interpretation of the results.

13. Figure 2.41 shows Bouguer gravity values at 30 m intervals. The following methods of analysis are suggested:
    (i) Remove the regional by drawing contours and graphical smoothing.
    (ii) Remove the regional by gridding.
    (iii) Calculate the second derivative.
    (iv) Carry out downward continuation by any method you know.

    Compare the results achieved with the different methods and consider their relative advantages and limitations. Interpret the residual anomaly or anomalies, if any, and calculate the excess mass. Is the section large enough to give reasonable results?

Table 2.7.

Stn	L20N (mGal)	L16N (mGal)	L10N (mGal)	L2N (mGal)
4W	45.38	45.71	46.10	—
3W	45.47	45.94	46.10	46.43
2W	45.68	45.90	46.40	46.48
1W	45.79	45.97	46.22	46.60
BL	45.91	45.93	46.27	46.68
1E	46.09	46.14	46.31	47.00
2E	46.21	46.42	46.55	47.09
3E	46.08	46.40	46.72	47.00
4E	46.54	46.53	46.80	47.12
5E	46.62	46.75	46.66	47.50
6E	46.91	46.87	46.61	47.61

Table 2.8.

Line 0			Line 2S		
Stn	H.I. (m)	Elev. (m)	Stn	H.I. (m)	Elev. (m)
53	0.46	6.76	53	0.46	8.03
52	0.43	6.99	52	0.44	7.85
51	0.49	7.08	51	0.43	8.20
50	0.47	5.95	50	0.43	8.50
49	0.51	4.73	49	0.46	8.75
48	0.53	4.68	48	0.46	8.91
47	0.53	6.00	47	0.47	8.61
46	0.48	6.42	46	0.46	8.36
45	0.50	6.40	45	0.40	8.64
44	0.48	6.75	44	0.41	9.03
43	0.47	7.20	43	0.43	9.06
42	0.50	6.64	42	0.42	8.41
41	0.46	5.82	41	0.45	8.02
40	0.39	5.96	40	0.44	7.65
39	0.45	6.21	39	0.48	7.62
			24	0.44	3.84
25	0.50	2.59	25	0.46	4.74
26	0.46	3.15	26	0.41	4.88
27	0.40	3.78	27	0.42	4.69
28	0.50	3.17	28	0.42	5.69
29	0.43	1.96	29	0.45	6.15
30	0.45	1.31	30	0.46	6.03
31	0.40	2.22	31	0.42	6.51
32	0.43	0.00	32	0.42	7.01
33	0.42	1.04	33	0.45	6.89
34	0.48	1.55	34	0.45	6.34
35	0.47	2.50	35	0.44	5.39
36	0.47	3.00	36	0.45	6.58
37	0.49	4.06	37	0.46	7.80
38	0.47	5.38	38	0.46	7.67
39	0.48	6.21	39	0.45	7.62
53	0.45	6.76	53	0.43	8.03

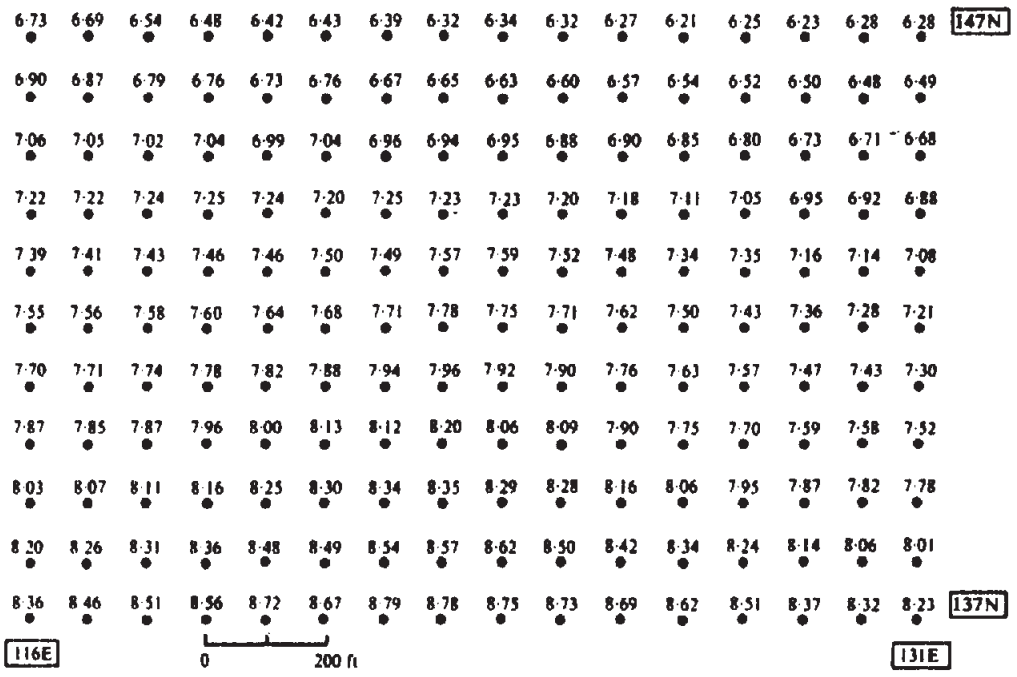

Figure 2.41. Bouguer gravity values on 30 m grid; values in milligals.

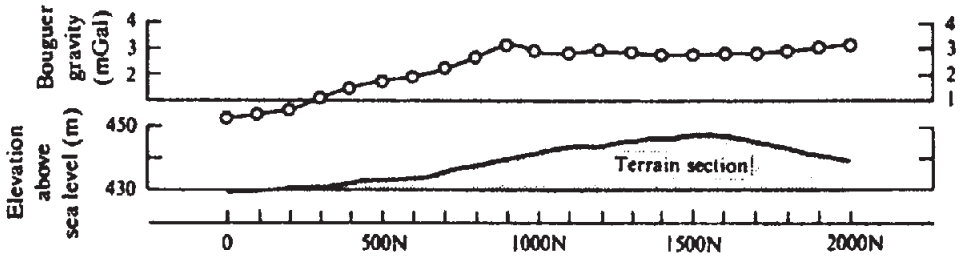

Figure 2.42. Bouguer gravity and topographic profiles, East Africa.

14. A topographic section and Bouguer gravity profile over a long east–west ridge are shown in Figure 2.42. Without other information, is it possible to answer the following questions with assurance?
    (a) Was a terrain correction taken out in reducing the gravity readings?
    (b) Is a terrain correction necessary?
    (c) Is the gravity profile essentially a reflection of the topography?
    (d) Is a regional gravity effect present that is independent of the topography?
    (e) Assuming there is a gravity anomaly caused by a subsurface structure, can you locate it and estimate its approximate section? (As an aid to making this interpretation, it would be very helpful to replot the gravity profile on an expanded vertical scale.)
15. Figure 2.43 is a Bouguer gravity contour map of the area whose topography is shown in Figure 2.39. The geology is sedimentary, with sandstone and limestone beds that are known to be over 5,000 ft thick a few miles to the west. Within the survey area the limestone–sandstone contact can be seen at the bottom of the hill just west of the base line. The limestone bed extends east from this contact at surface and appears to be less than 50 ft thick; because it does not continue west under the hill, a fault is indicated. Under normal circumstances, the sandstone would have the lower density; but in this area, because the limestone is thin and because there are underground streams flowing in it, the density contrast is probably insignificant and may even be in the opposite sense.

    Problem 7, with which Figure 2.39 is connected, was an exercise in making terrain corrections in rugged ground. Preparation of the map in Figure 2.43 required more than 15 man-days of work, most of it spent on terrain corrections for about 400 gravity stations. The end result is a gravity map that appears to be a fair reproduction of the topography.

    Do the two maps, Figures 2.39 and 2.43, resemble each other in spite of the elaborate terrain correction or because of it? If the latter is

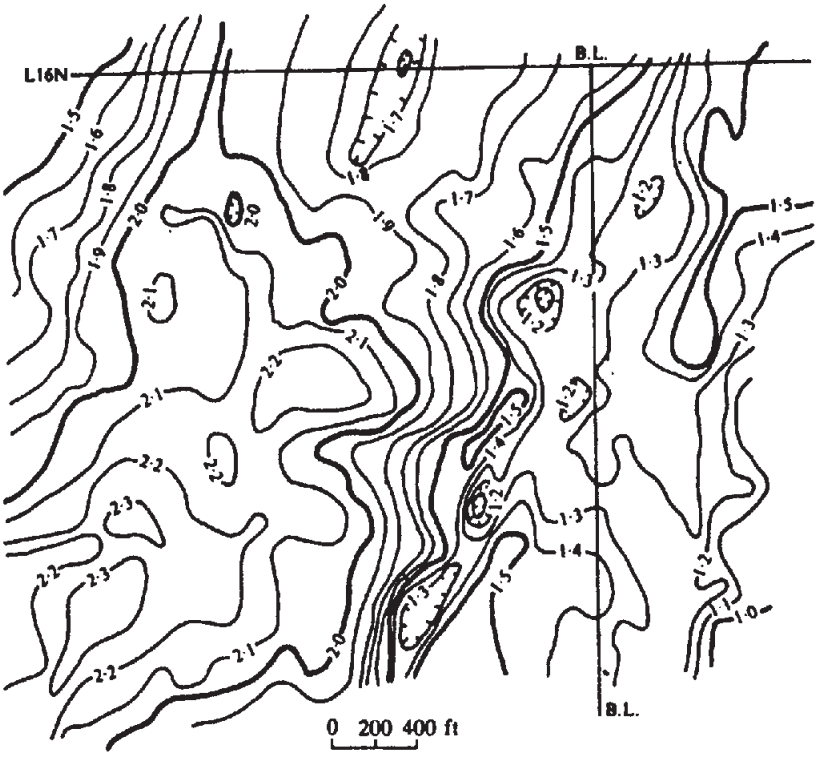

Figure 2.43. Bouguer gravity contours, eastern Nova Scotia; C.I. = 0.1 mGal.

true, would this be a fundamental argument against carrying out gravity surveys in regions where the topography is highly irregular? On the other hand, if the anomalous gravity is not due to topography, how do you explain it?

16. The reduced gravity contours in Figure 2.44 show a portion of a large survey made over a base-metal property in southern New Brunswick. Remove the regional. Given that there are ore-grade sulfides in the area, interpret the residual and estimate the excess mass.
17. Figure 2.45 shows residual Bouguer gravity across a three-dimensional structure of positive density contrast in the St. Lawrence lowlands east of Montreal. The contours are approximately circular. Drill logs from gas and oil exploration holes in the vicinity have indicated flat-lying sedimentary beds to a depth of over 4,000 ft. The maximum density contrast among the different sediments is not greater than 0.2 g/cm^3 and generally is closer to 0.1. Density of the Precambrian basement rocks is not known, but they are probably denser than the average sediments by 0.25–0.30 g/cm^3.

    To interpret this anomaly, first consider the maximum gravity combined with the maximum slope of the flanks, with respect to the known depths and density contrasts in the area. This will indicate an approximate depth to the source. Then attempt to match the profile with a simple shape, such as the sphere, rod, cylinder, and so forth. (Note that it is possible to simulate a pillbox-type of structure by taking the difference between the gravity effects of two long cylinders with their tops at different depths.)
18. On the portion of the Bouguer anomaly map shown in Figure 2.46, the most negative values are found in the lower left corner. (The numerical values shown are with respect to an arbitrary datum.)

    (a) A large fault strikes N20°W just east of AUS. Examine the shape of the fault anomaly by drawing the profile *A'A*.

    (b) For a simple fault model, the point where the fault's gravity expression is half its maximum value locates the fault. What difficulties are encountered in the practical application of this rule? Another rule is that the fault is located at the inflection point on the fault profile. Locate the fault on this profile by applying these rules. What does the asymmetry of the fault profile indicate?

    (c) The half-width rule states that the depth to the midpoint on a fault is equal to the distance between the points on the fault's gravity profile, where the fault's gravity expression is $\frac{1}{4}$ and $\frac{1}{2}$ (or $\frac{1}{2}$ and $\frac{3}{4}$) of its maximum expression. What depth does this give for this fault? What difficulties are encountered in the practical application of this rule?

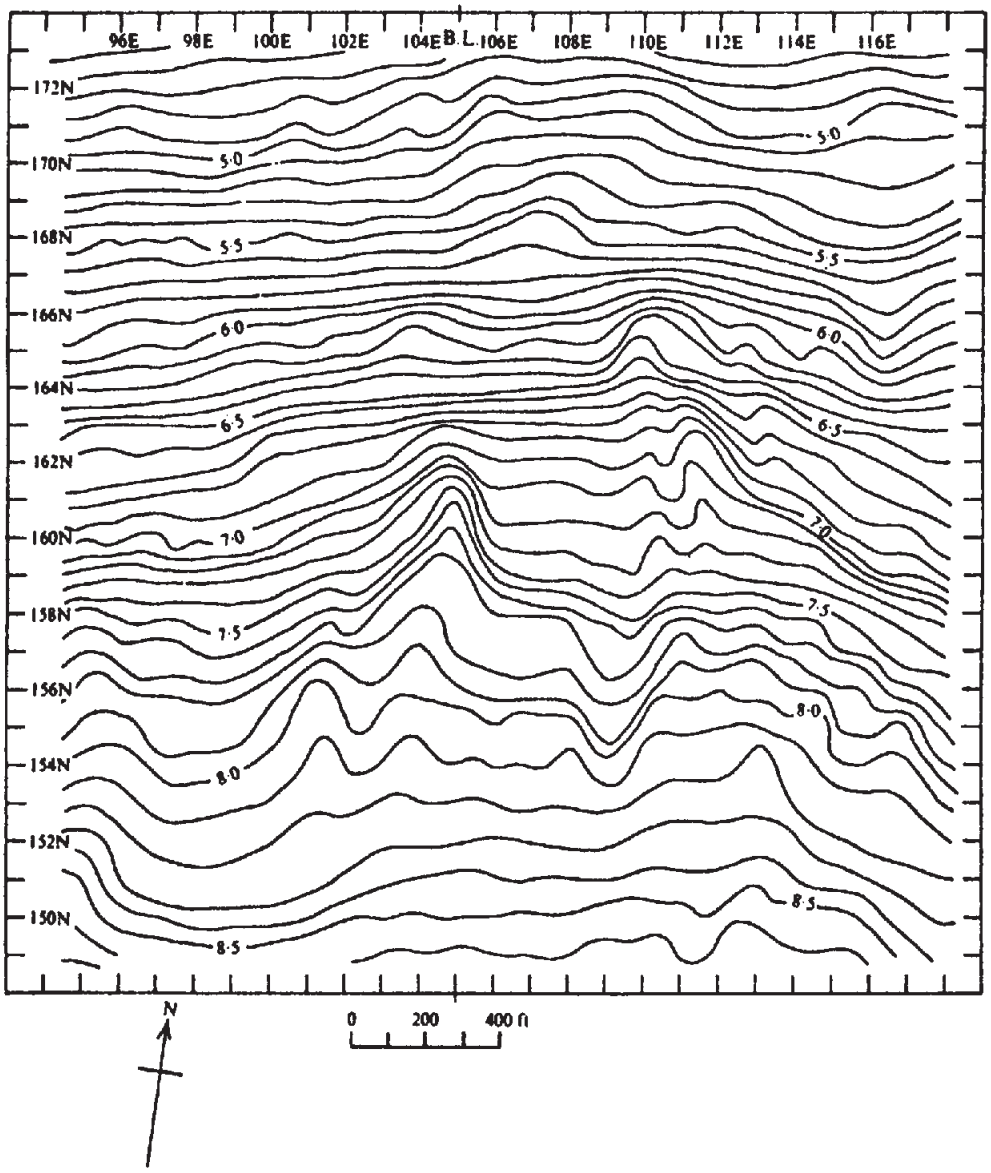

Figure 2.44. Bouguer gravity contours, southern New Brunswick; C.I. = 0.1 mGal.

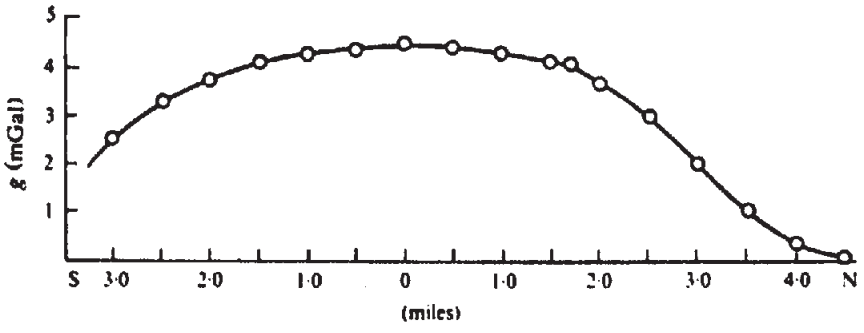

Figure 2.45. Residual gravity profile over three-dimensional structure, St. Lawrence lowlands.